A Hybrid Deep Learning Model for Layer-Wise Melt Pool Temperature Forecasting in Wire-Arc Additive Manufacturing Process

PAVAN KUMAR NALAJAM AND RAMESH VARADARAJAN, (Member, IEEE)

School of Electrical Engineering, Vellore Institute of Technology (VIT), Vellore 632014, India

Corresponding author: Ramesh Varadarajan (vramesh@vit.ac.in)

ABSTRACT Melt pool temperature contains abundant information on metallurgical and mechanical aspects of products produced by additive manufacturing. Forecasting melt pool temperature profile during a process can help in reducing microstructural porosity and residual stresses. Although analytical and numerical models were reported, the performance of these are questionable when applied in real-time. Hence, we developed data-driven models to address this challenge, for continuous forecasting layer-wise melt pool temperature using a hybrid deep learning technique. The melt pool temperature forecasting by the proposed CNN-LSTM model is found to be better than other benchmark models in terms of accuracy and efficiency. The model results have shown that combining CNN and LSTM networks can extract the spatial and temporal information from the melt pool temperature data. Further, the proposed model results are compared with existing statistical and machine learning models. The performance measures of the proposed CNN-LSTM model indicate a greater potential for in-situ monitoring of additive manufacturing process.

INDEX TERMS Wire-arc additive manufacturing, melt pool temperature forecasting, deep learning, CNN, LSTM, statistical learning, machine learning.

NOMENCLATURE

x_i	Melt pool temperature vector with length i.
y_{ij}^l	Convolved output of lth layer.
σ	Activation function.
b_j^l	Bias for the jth feature map of lth layer.
ω	Kernel width.
m	Index value of filter.
p_{ij}^l	Pooling operation of lth layer.
T	Stride.
R	Pooling size.
i_t	Input gate.
c_t	Control gate.
f_t	Forget gate.
o_t	Output gate.
h_t	Hidden state.
W_i, W_f, W_o	Weight matrix of input, forget and output gates.
p_t	Output of pooling layer at time t.
b_i, b_f, b_o	Bias vectors of input, forget and output gates.
$O(..)$	Big O notation.
d	Number of convolutional layers.
nf	Number of filters.
s	Spatial size of filter.
q	Spatial size of feature map.
e	Number of epochs.
N	Total number of samples

The associate editor coordinating the review of this manuscript and approving it for publication was Rosalia Maglietta.

I. INTRODUCTION

Metal additive manufacturing (AM) processes of directed energy deposition (DED) offer numerous possibilities for producing complex parts in aerospace and automotive industries without design constraints. Compared to traditional manufacturing, AM offers four key advantages that include design flexibility, sustainability, higher accuracy and efficiency, and faster production cycles. In recent years, AM techniques have brought key transformations in aerospace and automotive industries. For example, Boeing used more than 600 additively manufactured parts in its aircraft 777X. The BMW group has produced over 300,000 additively manufactured parts in just one year [1].

Wire arc additive manufacturing also known as DED-arc produces near net-shaped parts by melting wire feedstock with an electric arc. The electric arc heat source has many processing advantages over other heat sources such as electron beam and laser [2]. Plasma arc-based AM techniques offer wide ranges of power densities and metal deposition rates with high efficiency and flexibility [3]. Cold metal transfer (CMT), which is an arc welding technology has shown significant potential in metal additive manufacturing of components. CMT is a relatively new technique that is characterized by many advantages including low thermal heat input and high deposition rates [4]. A substantial amount of research was reported on application of CMT for additive manufacturing in recent times. The effects of various arc modes in CMT process on porosity was reported [5]. Fang *et al.* studied the evolution of microstructures and mechanical behaviour of aluminium alloys [6]. Ryan *et al.* studied the influence of build parameters and wire batch on porosity of CMT based additively manufactured aluminum alloy [7]. There are still some critical challenges such as porosity and voids, particularly for producing parts with aluminium (Al) alloys, that need to be addressed before AM technologies take up widespread adoption in the manufacturing sector [8]. The possible causes of microstructural defects are the lack of fusion, insufficient heat, entrapped gases and rapid solidification [9]. Investigating melt pool temperature profile such as temperature distribution and heat flow mechanism reveals information on most of the possible causes of microstructural defects. The melt pool temperature profile contains abundant information and that can be used to reduce the porosity defects and voids of the Al parts manufactured by AM [10].

The melt pool in wire-arc additive manufacturing (WAAM) refers to the vicinity of electric arc and molten material interface where the wire feed stock is melted and form spherical molten metal droplet. Temperature variations can significantly affect the evolution of porosity in final products. In comparison to powder-bed AM, very few reports are available on WAAM that discuss the process parametric effects and melt pool temperature variations on porosity formation [11]. This is due to the complex and dynamic nature of arc. The metal deposition using an electric arc imposes thermal cycles not only on solidified material and substrate, but also on the previous deposited layers. The imposed thermal cycles result in partial melting of previous layers below the deposited layer, up to 4 layers, creating non-isothermal heat treatment. This heat effect leads to expansion and contraction of deposited metal and subsequent generation of residual stresses in the deposited structures [12], [13]. Also, the nucleation and dissolution of eutectic phases of alloys during solidification and melting processes, resulted in the formation of pores. The degree of residual stresses and porosity is a function of temperature distribution and thermophysical properties [14]. Therefore, melt pool temperature monitoring and controlling helps in achieving desired microstructural and mechanical properties of the WAAM components. This study aims to develop data-driven models for continuous forecasting of layer-wise melt pool temperature in order to control the microstructural defects.

The temperature profile in the melt pool can be monitored using various types of sensors, such as pyrometers, thermocouples and infrared (IR) radiation. Thermocouples have limitations in being used for in-process monitoring, as they need contact with the parts to monitor temperature [15]. However, IR cameras and pyrometers are feasible for monitoring temperature of a process without contact. With the recent advancements in instrumentation, IR cameras are capable of obtaining temperature data with a sampling rate up to 100kHz. The temperature profile during DED processes have been extensively studied with regard to physics involved and data – based models. Physics-based models can be broadly categorized into numerical and analytical methods. Analytical temperature models of DED involve solving of closed form welding heat transfer equations using boundary conditions [16]. Cadiou *et al.* proposed a 3D heat transfer model for wire-arc additive manufacturing process [17] The major limitations of analytical models are their general applicability and failure to address the uncertainties of thermophysical properties. Finite element method (FEM) is a numerical method of modelling of temperature profile. The accuracy of these models is questionable due to the lack of process knowledge. Also, the performance of numeral models depend highly on boundary conditions, element types and meshing schemes [18]. In contrast to physics-based models, data driven models offer many advantages and can model highly non-linear processes such as melt pool formation with good accuracy and efficiency. Further, data-driven models require only limited knowledge of process and physics involved [19]. Some studies were reported on defect detection from melt pool temperature profile during DED process by using classical machine learning and deep learning techniques [20]. Recently, a study was performed on prediction of melt pool temperature during DED process using machine learning [21]. However, there are very few papers reported on controlling and monitoring of temperature profile during DED process. This research gap can be effectively addressed using deep learning time series forecasting techniques. The main idea is that deep learning time series models can forecast layer-wise melt pool temperature during DED process with higher accuracy and faster response times.

In most of the time series data, correlations exist between observations. A standard neural network considers all the observations as independent, that leads to an erroneous inference. With recent developments in deep learning techniques, many special types of neural networks have been introduced to deal with noisy and correlated time-series data and can lead to more accurate forecasting. Though some ARIMA family models can address the correlations in time series, they do not consider the effects of spatial dependencies. Traditional time series models such as ARIMA and SARIMAX works well when seasonal and trend components are known. However, in real-time manufacturing, both seasonal and trend components change with regard to process

parametric variations. These parameters need to be changed for each simulation when using traditional time series models. Among various deep learning techniques, convolutional neural networks (CNN) and recurrent neural networks (RNN) are most popular, efficient and widely used neural networks. Long short-term memory (LSTM) networks are special type of RNN that deals with long-term sequential dependencies very effectively [22]. CNNs are traditionally used for image classification and recognition and do not account for sequential dependencies. However, when dealing with time-series data, the main advantage of CNN is dilated convolutions [23]. The CNN allows neural network to extract relationships between different observations in time series that accounts for spatial dependencies. Therefore, combining the CNN and LSTM models to exploit the benefits of spatial and temporal information of time series could improve the forecasting performance [24]. In this paper, a hybrid deep learning model is proposed to forecast the layer-wise melt pool temperature during DED process. The proposed CNN-LSTM model performance is evaluated using RMSE, MAE and MAPE, and also compared the performance metrics with traditional statistical, machine learning and deep learning models. The major contributions of this study are as follows:

- This paper proposes a hybrid CNN-LSTM network to forecast layer-wise melt pool temperature during the DED process in order to control and monitor the temperature distribution.
- It analyses the model feasibility for real-time monitoring of additive manufacturing process.
- The proposed model has been compared with classical methods of time series forecasting.

The rest of this paper is structured is as follows. In section 2, background knowledge of melt pool temperature modelling is presented and related state-of-the-art CNN-LSTM network-based models for a variety of applications is reviewed. Section 3 provides the details of experimentation and data collection. In section 4, methodology of the network is illustrated in detail. Results obtained are provided in section 5, comparison of forecasting results are demonstrated in section 6 and Finally, major conclusions of this study are provided in section 7.

II. RELATED WORK
A. THERMAL SENSING
The heat flow during DED is a quasi-stationary process, with respect to moving arc heat source. To be specific, the temperature distribution in the melt pool surface does not change with time except for initial and final transients [34]. Thus, thermal sensing techniques are an effective way of monitoring DED. Thermal methods are fast when compared to other non-destructive testing methods such as ultrasonics, for quality monitoring of process. It is a very feasible process and allows rapid results during manufacturing of parts. Every object emits electromagnetic radiation from its surface proportional to its temperature. This intrinsic radiation

associated with temperature is called infrared radiation and can be used for temperature measurement. Khanzadeh et al. [25] developed a thermal sensing system with a pyrometer and IR camera to analyse the temperature changes in laser-based AM process. The melt pool images were analysed using self-organizing maps (SOM). The proposed methodology was able to detect the porosity locations with an accuracy of 85%. Sreedhar et al. [26] developed an online monitoring system for gas tungsten arc welding (GTAW) using thermal images. The authors noticed a distinctive pattern at the defective locations over non-defective areas. Mireles et al. [27] proposed in-situ monitoring technique for defect detection. The authors mapped the results obtained from computed tomography (CT) and layer-wise thermography to find defects. Krauss et al. [28] developed a model to detect flaws in selective laser melting (SLM) process using thermography measurements of molten pool.

B. MELT POOL TEMPERATURE MODELLING
Analytical models of temperature distributions of wire-based DED have been extensively studied in literature. Rosenthal [29] and Rykalin [30] developed analytical models to calculate weld dimensions from temperature distributions of moving point heat source. Several analytical models have been developed for additive manufacturing processes. Pinkerton and Li [31] derived a model that is applicable for low travel speeds from Rosenthal equations. Beuth and Klingbeil [32] developed analytical model to predict melt pool length. However, the performance of analytical models for in-situ monitoring of additive manufacturing processes is questionable. Also, physics-based analytical models cannot address the uncertainties and variances that occur during a process. Numerical models of additive manufacturing processes have been shown to be efficient in predicting thermal profile given all the boundary conditions. Hejripour et al. [33] developed a fluid flow and heat transfer model for WAAM process. The author predicted the shape of deposited material for single layer using an arbitrary Lagrangian-Eulerian method. Kou [34] proposed a 3D model of WAAM process to predict material dimensions and temperature distributions from machine operating parameters. The model was developed by taking into account electromagnetism, fluid flow and heat transfer. Zhang et al. [35] derived a relationship between thermal profile and microstructures evolution in melt pool by using finite element method. Numerical models have some important limitations that include high computational costs, oversimplified assumptions and various meshing schemes.

Data-driven models of melt pool temperature during DED processes have recently gained a considerable amount of interest among the researchers. Khanzadeh et al. [36] detected porosity in additively manufactured samples from melt pool temperature profile using supervised machine learning techniques. The extracted features of melt pool images were fed to k-nearest neighbor (kNN) method and the predicted results were in good coherence with experimental results. Mozaffar et al. [37] estimated high-dimensional

thermal profile in DED process using the large amount of data obtained from the fine element code. A gated recurrent unit (GRU) model was used to predict the temperature profile and the results of model shown high accuracy. However, general applicability of these models are questionable due to the stand-alone models used. For example, in CMT technology, the process behaviour leads to a seasonal trend and that need to be addressed during forecasting. The stand-alone models may fail to understand the process profoundly.

C. APPLICATIONS OF CNN-LSTM MODELS

In recent years, many researchers have combined CNN and LSTM model to exploit the benefit of spatial and sequential features in variety of applications. Huang *et al.* proposed a particulate matter (PM2.5) concentration forecasting system by combining CNN and LSTM networks. Further, the authors evaluated model using MAE and RMSE and concluded that the performance of model is better than the traditional machine learning models [38]. A similar work was reported for forecasting PM2.5 using CNN-LSTM network [39]. Kim *et al.* proposed a hybrid CNN-LSTM model to predict the residential electrical energy consumption and analysed the various variables that affect the prediction of energy consumption [40]. Rehman *et al.* improved the accuracy of movie reviews sentiment analysis [41]. A considerable amount of research has been conducted in the field of natural language processing using CNN-LSTM networks [42], [43]. In the field of medical image processing, Petmezas *et al.* developed an automatic atrial fibrillation detection system from electrocardiogram (ECG) signals using CNN-LSTM network with a high sensitivity and specificity [44]. Vidal *et al.* used CNN-LSTM network to predict the future volatility of gold prices and the performance is compared with the other classic models [45]. The CNN-LSTM network proved to be a potential technique in forecasting time series and opening up new possibilities in various areas of applications.

III. METHODOLOGY

The main idea of this research is the development of hybrid deep learning model for forecasting melt pool temperature during additive manufacturing process by exploiting the benefits of convolutional and long short-term memory networks. Convolutional networks are special kind of neural networks for processing grid-like topology, such as time series (1D) and images (2D) [46]. They have been effective for learning spatial information of time series. Whereas, LSTM networks are tremendously successful in identifying short and long-term dependencies. Thus, the proposed CNN-LSTM model for forecasting melt pool temperature combines the advantages of both CNN and LSTM networks. The hybrid model consists of two components: The first component consists of convolutional and pooling layers, in which features are developed from the internal representation of time series data, while the second component exploits the features generated by LSTM and dense layers. Each layer is briefly discussed in the following sections.

A. CONVOLUTION AND POOLING LAYERS

Figure 1 shows the 1D convolutional operation. Convolutional networks have advantages such as sparse interactions and weight sharing over multilayer perceptron networks. This effectively reduces the number of parameters used in model computation. The output s in Fig. 1 is the convolved output of three inputs, that is, the output is only affected by the kernel width.
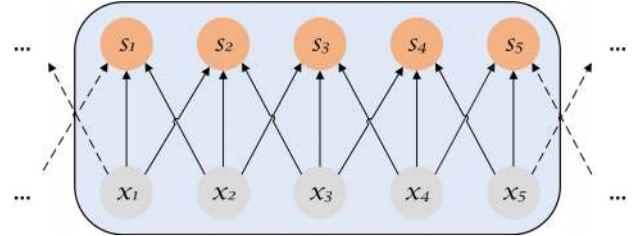

FIGURE 1. Schematic of 1D convolutional operation: s is formed with kernel size of 3.

The CNN layer receives step-wise melt pool temperature variables as inputs. The inputs must be represented in a structured matrix form, since the technique is originally developed for grid-like topologies. The convolutional filter consists of coefficient values in a matrix form and can be considered as a tiny window. This window slides through input matrix performing convolution operation. The output layer of CNN provides extracted feature information to several hidden layers and LSTM network. Each hidden layer of CNN consists of an activation, convolution and pooling layers respectively. Convolution layer performs convolution operation on an input sequence. This operation reduces the number of parameters and leads to a deeper CNN-LSTM network. If x_i, where $i = 1, 2, \ldots, n$ is the input vector of melt pool temperature steps and n is the normalized unit window, then the resultant output vector, y_{ij} of the lth convolutional layer is as follows.

$$y_{ij}^l = \sigma \left(b_j^l + \sum_{m=1}^{M} w_{m,j}^l x_{i+m-1,j} \right) \quad (1)$$

where σ is the activation function, b_j^l is the bias for j^{th} feature map, w is the kernel weight, and m is the index value of filter. The output of each neuron cluster is mapped to the next layer by pooling operation. This helps in reducing the number of computational parameters and cost. The pooling layers produce summarized values of the convolved features. The max-pooling for predicting melt pool temperature utilizes the maximum value of a convolved matrix, which adjusts overfitting issue also [47]. The max pooling layer operation is represented in Eq. (2), where T is the stride and R is the size of pooling. The equation performs pooling operation on the previous convolutional layer.

$$p_{ij}^l = max_{r \in R} \left(y_{i \times T + r, j}^l \right) \quad (2)$$

B. LSTM LAYER

LSTMs are a special kind of artificial RNN architecture that are capable of learning long-term dependencies of a time-series data [40]. The issue in long-term memory of traditional RNNs was successfully addressed by LSTMs for sequential data. The hidden layers of these models employ cyclic connections which store useful information from previous states. Further, LSTM networks effectively tackle vanishing gradient problem of RNNs by storing useful information and discarding unnecessary information. Thus, LSTM networks provide better performance over classical RNN models. The LSTM layer of CNN-LSTM network stores the important information of melt pool temperature distribution that is extracted by the CNN layer. The output of LSTM layers is the resultant of consolidated memory units by storing long-term memory of previous hidden states. These memory cell units are able to extract and analyse temporal information of sequential data. The output information of CNN layer is fed to the gated units of LSTM network. For forecasting melt pool temperature time-series data, LSTM networks are well suited, by addressing the vanishing and explosive gradient problems that occur in traditional recurrent neural networks.

The three-gate unit mechanism shown in Fig. 2, represents the working of each memory cell at a particular run. The gate unit is a combination of input, forget and output gate. The input gate along with control gate c_t, controls the information that has to be stored in the memory cells at given time t. The forget gate f_t controls the previous intervals information and decides which information has to be kept on memory cell, while output gate o_t decides which information could be used for the memory cell output. Equations. (3) – (5) describes the operation of a LSTM unit.

$$i_t = \sigma \left(W_{pi} p_t + W_{hi} h_{t-1} + W_{ci} * c_{t-1} + b_i \right) \quad (3)$$

$$f_t = \sigma \left(W_{pf} p_t + W_{hf} h_{t-1} + W_{cf} * c_{t-1} + b_f \right) \quad (4)$$

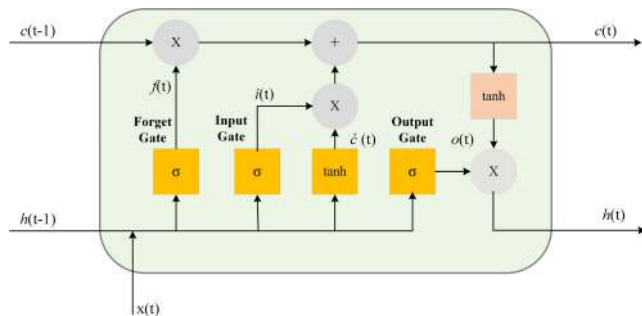$$o_t = \sigma \left(W_{po} p_t + W_{ho} h_{t-1} + W_{co} * c_t + b_o \right) \quad (5)$$

FIGURE 2. LSTM network structure.

Equations (6) and (7) provides the cell and hidden (h_t) states derived from the input, forget and output gates. σ is an activation function, and W and b represents weight matrix and their associated biases. The output, p_t of pooling layer at

time t contains crucial information of melt pool temperature time-series data and passed to an LSTM cell.

$$c_t = f_t * c_{t-1} + i_t * \sigma \left(W_{pc} p_t + W_{hc} h_{t-1} + b_c \right) \quad (6)$$

$$h_t = o_t * \sigma(c_t) \quad (7)$$

The output of LSTM layer is fed to the fully connected layer. This can be used to generate melt pool temperature forecasting over a certain interval of time. Here, we forecasted the melt pool temperature for the final layer while producing thin-wall structures.

C. CNN-LSTM ARCHITECTURE

The proposed CNN-LSTM architecture is shown in Fig. 3. The input of the network is melt-pool temperature measurements for nine layers of deposition. The output of the network is forecasted values of melt pool temperature for 10th layer. The network in convolution and pooling layer consists of two Conv1D layers, two max-pooling layers and one time-distributed layer. Subsequently, features extracted from the convolutional layer is passed through LSTM layer, followed by dense layers. Rectified Linear unit (ReLu) is used as an activation function for convolutional layers. Though there are other modified activation functions, ReLu shown to be effective for melt pool temperature forecasting with no sign of exploding or vanishing gradient problems. To avoid overfitting during training, dropout was used. Dropout is a widely used technique to avoid overfitting that randomly ignores the neurons during training phase. Further, number of epochs was carefully selected to avoid overfitting and same number of epochs were used for each sample. The design parameters of CNN-LSTM model are shown in Table 1. This table provides the information on number of filters used, kernel width, stride window and the number of parameters for each layer.
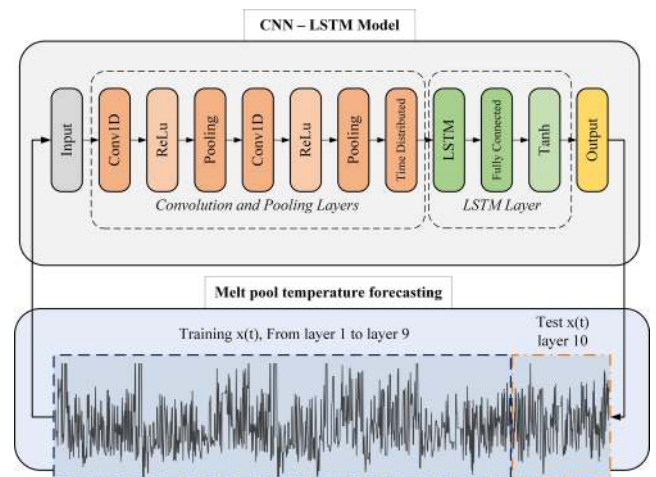

FIGURE 3. The architecture of proposed CNN-LSTM network.

The complexity of CNN-LSTM can be calculated by calculating the time complexities of the convolutional layers and the LSTM layer individually. The complexity of

TABLE 1. The proposed CNN-LSTM architecture.

Type	Kernel Size	Stride	Params #
Convolution (filters=64)	(3,1)	1	256
Activation (ReLu)	-	-	0
Max Pooling	(2,1)	2	0
Convolution (filters=64)	(3,1)	1	12352
Activation (ReLu)	-	-	0
Max Pooling	(2,1)	2	0
Time Distributed	-	-	0
LSTM (nodes=100)	-	-	142800
Activation (Tanh)	-	-	0
Dense (100)	-	-	10100
Dense (1)	-	-	101
Total number of parameters	-	-	165609

CNN layer is estimated as $O(\sum_{l=1}^{d} n_{l-1}.s_l^2.n_l.q_l^2)$, where d, n_{l-1}, s_l and q_l are the number of convolutional layers, number of filters in l^{th} layer, spatial size of filter and spatial size of output feature map respectively [48]. The complexity of the convolution layer grows quadratically with kernel width, number of kernels and cache unfriendly memory access [49]. Whereas, input length does not affect storage requirements of LSTM network, local in space and time [50]. Thus, the overall complexity of LSTM network is $O(\omega)$, where ω corresponds to number of weights. Therefore, overall complexity of CNN-LSTM network is the sum of complexities of CNN and LSTM layers and can be expressed as: $O\left((\sum_{l=1}^{d}(n_{l-1}.s_l^2.n_l.q_l^2) + \omega).i.e\right)$, where i is the length of input and e is the number of epochs.

IV. DATA COLLECTION
A. MATERIALS AND EXPERIMENTAL SETUP
Thin-walled structures are produced with aluminium alloy 4043/AA4043 wire with diameter of 2 mm and melting temperature is in range of 573°C and 632°C. The material is deposited on aluminium alloy 6061/AA6061 substrates. Nominal chemical compositions of AA6061 and AA4043 used in this study are shown in Table 1.

Thin-walled structures were produced using a CMT 7000 VR power source. Fig. 3 illustrates the schematic of directed energy deposition platform used in this study. The wire feedstock was thoroughly cleaned and dried before experimentation. The substrate was firmly clamped onto the workbench and movement of welding torch in X and Y directions was controlled by a linear actuation system. The wire is deposited in single pass layers along the Z direction and the alternating layers are deposited in the opposite direction.

A total of nine samples were produced by varying current and speed levels in order to collect the temperature data. Other parameters were maintained constant throughout the metal deposition process. Table 2 shows the process parametric levels used in this study. Each parameter has three levels and a sample of thin-walled structure has ten layers in total. The length, height and width of each sample are 80 ± 2 mm, 30 ± 2 mm and 3 ± 0.5 mm respectively.

TABLE 2. Nominal chemical composition of materials used in this study.

Material	Al (%)	Si (%)	Mg (%)	Cu (%)	Fe (%)	Mn (%)	Zn (%)
AA6061	97.59	0.890	0.86	0.29	0.33	0.025	0.007
AA4043	93.05	6.0	0.05	-	0.8	-	0.10

B. MELT POOL TEMPERATURE MEASUREMENTS
The melt pool temperature data of wire feedstock was continuously monitored and recorded using a Fluke Ti480 infrared thermal imaging camera. A high-resolution video (480×360 pixels) was captured for each sample using an IR camera with a frequency of 9 Hz. The temperature of the IR camera was adjusted in the range of 10°C to 1600°C. The emissivity value of camera was adjusted to 0.60. The layer wise temperature data of layer 1, 3, 5, 7, 9 and 10 are shown in Fig. 4.

The data collected from nine samples each with ten layers was recorded. The data of first nine layers was used to model the time-series models. The last layer (10th layer) data of each sample was forecasted and the same has been validated with performance metrics. All the forecasting experiments were performed using a computer with the specifications as follows: 24 GB graphics card (NVIDIA TITAN RTX), 64 GB random access memory (RAM), Intel i9 processor and Windows 10 operating system. The melt pool temperature forecasting results for last layer of thin-walled structure were simulated with faster response times. All the models were implemented using Python 3.7 and the libraries used are *Statsmodels*, *Scikit − Learn* and *Keras*.

The melt pool temperature of wire-based directed energy deposition process was continuously recorded using an IR thermal camera. The diameter of melt pool was in the range of 1.5 mm to 2.0 mm. The peak temperature recorded in the region was taken as melt pool temperature. The melt pool temperature distribution of sample 1 for ten layered thin-walled structure is shown in Fig. 6. Layer 1 represents the ground layer and the 10th layer indicates roof layer. The average temperature recorded in each layer of sample 1 is shown in Table 3. The mean temperature tends to increase with each layer, due to the heat accumulation effect. The dwell time was maintained at a constant value for all the experiments. Further, temperature observed during dwell time is around 455°C and was constant for all the layers. The dwell time melt pool temperature value was omitted during modelling process. The temperature fluctuations persisted during each layer as can be clearly seen in Fig. 6. The temperature fluctuations are mainly due to the current cycling phases of CMT process and material's varying emissivity during the DED process. The melt pool temperature is plotted against the time indices by removing dwell time into consideration. The deposition time of each layer was made to remain constant. Fig. 7 shows the effects of varied process parameters, current and speed on the melt pool temperature profile of thin-walled structures. Each point on the line plots represent the average recorded melt pool temperature of that corresponding layer on X-axis. The temperature in Figs. 7(a) and 7(b) increases gradually from one layer to the adjacent layer. This is attributed to the heat
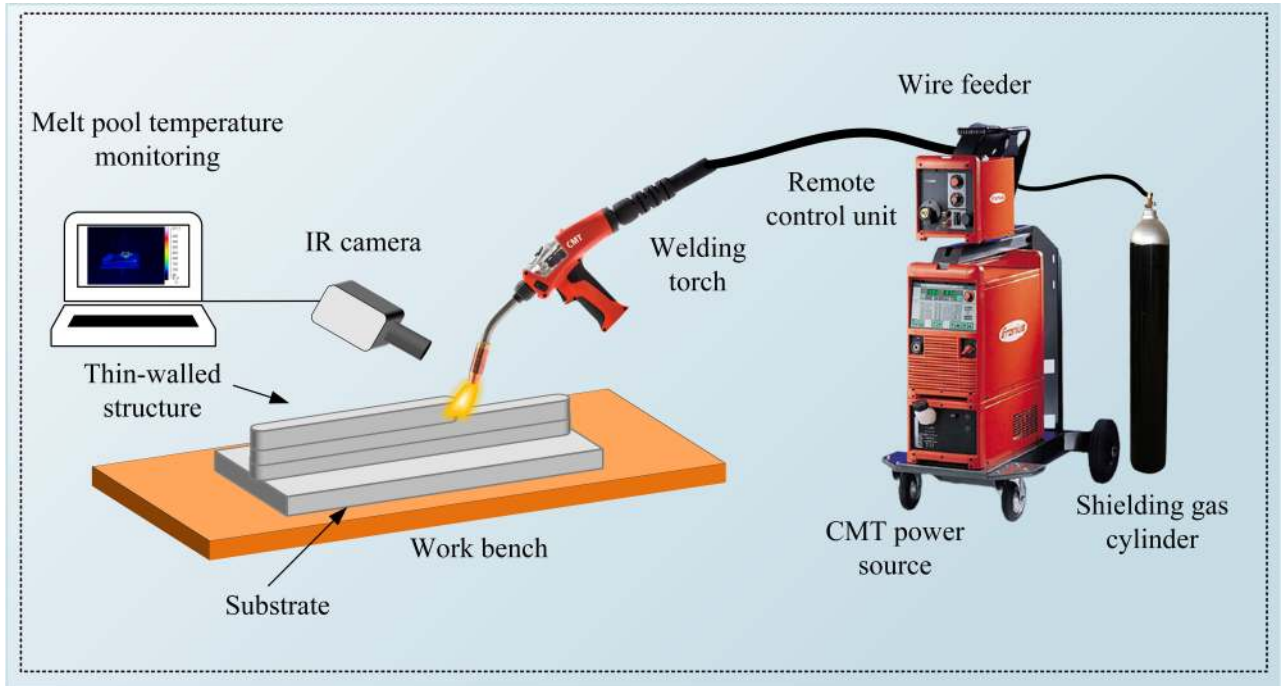
FIGURE 4. Schematic of directed energy deposition platform using cold metal transfer technology.

TABLE 3. Process parameters and their associated average melt pool temperature.

S.No.	Current (A)	Speed (mm/s)	Average melt pool temperature (°C)
1	50	5	674.22
2	50	7.5	667.54
3	50	10	662.36
4	60	5	704.5
5	60	7.5	697.98
6	60	10	688.89
7	70	5	720.16
8	70	7.5	715.57
9	70	10	707.5

accumulation effect. The melt pool temperature increases with increase in the current level (Fig. 7(a)). Whereas, melt pool temperature decreases with increase in speed level and the same can be observed in Fig. 7(b). However, similar pattern of temperature variation is observed from layer to the adjacent layer and that holds true for both current and speed variations.

Fig. 6 shows the effects of varied process parameters, current and speed on the melt pool temperature profile of thin-walled structures. Each point on the line plots represent the average recorded melt pool temperature of that corresponding layer on X-axis. The temperature in Figs. 6(a) and 6(b) increases gradually from one layer to the adjacent layer. This is attributed to the heat accumulation effect. The melt pool temperature increases with increase in the current level (Fig. 6(a)). Whereas, melt pool temperature decreases with increase in speed level and the same can be observed in Fig. 6(b). However, similar pattern of temperature

variation is observed from layer to the adjacent layer and that holds true for both current and speed variations.

V. RESULTS

The performance of the proposed model for forecasting melt pool temperature is evaluated from various metrics. The statistical metrics are utilized to assess the performance of all time-series models. The following commonly used statistical metrics for performance evaluation of time-series models are used.

$$RMSE = \left[\frac{1}{N} \sum_{i=1}^{N} (\bar{x}_i - x_i)^2 \right]^{1/2} \qquad (8)$$

$$MAE = \frac{1}{N} \sum_{i=1}^{N} |\bar{x}_i - x_i| \qquad (9)$$

$$MAPE = 100 \times \frac{1}{N} \sum_{i=1}^{N} \frac{|\bar{x}_i - x_i|}{x_i} \qquad (10)$$

where x_i and $\bar{x}_i$ are the actual and forecasted values of melt pool temperature ranging from $i = 1, 2, 3, \ldots, N$. The performance metrics of various statistical, machine learning and deep learning models are summarized in Tables 4, 6 and 7 respectively.

The performance measures of proposed CNN-LSTM algorithm for all the experiments are provided in Table 4. The metrics for experiments with various process parameters remains almost same. This shows the model's good repeatability characteristics for forecasting melt pool temperature in wire arc additive manufacturing process. Fig. 8 shows the comparative
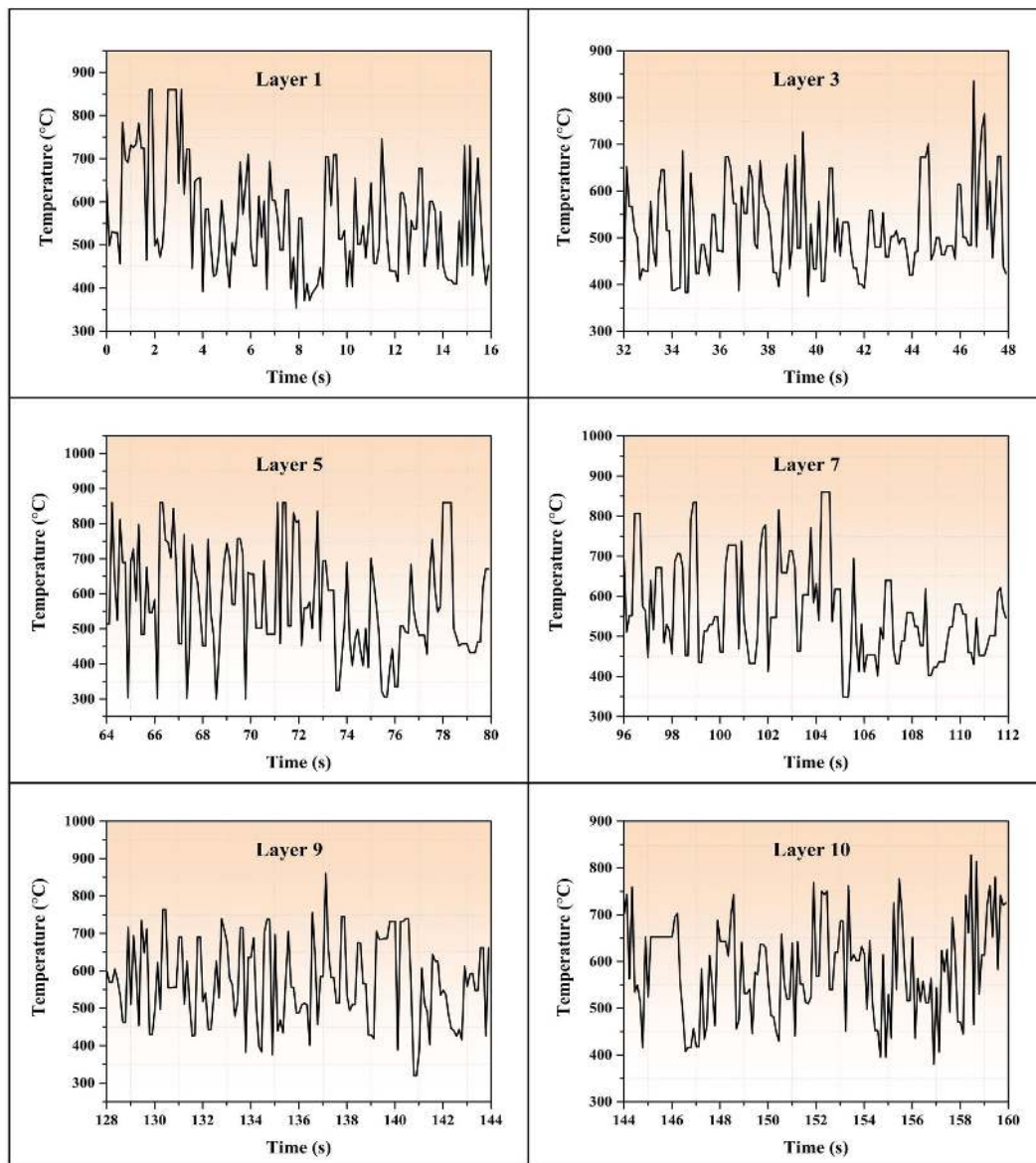
FIGURE 5. Melt pool temperature distribution in various layers of deposition.

plots of forecasted melt pool temperature values with actual values. All the forecasts are made for the roof layer (layer 10). The model exhibits robustness against noises. The average RMSE, MAE and MAPE of proposed CNN-LSTM model for sample 1 are 95.16, 75.43 and 12.19% respectively.

A. PERFORMANCE COMPARISON WITH TRADITIONAL METHODS

Among all the time-series forecasting models, statistical models still hold tremendous usability and considered as reference models for forecasting applications. Hence, in this study we compared the performance of the proposed model for melt pool temperature forecasting with both statistical and machine learning algorithms. The proposed CNN-LSTM model achieved the lowest mean square error over the

TABLE 4. Performance measures of the proposed CNN-LSTM model for melt pool temperature forecasting.

S.No.	RMSE	MAE	MAPE(%)
1	95.16	75.43	12.19
2	95.59	73.96	13.05
3	96.17	82.0	15.52
4	93.76	82.39	18.17
5	100.48	88.51	20.22
6	101.33	86.88	20.1
7	97.37	80.01	17.56
8	98.18	78.2	15.33
9	94.15	77.69	12.37

other models. Table 5 provides the model settings and hyper-parameters used for statistical and machine learning methods for forecasting melt pool temperature during WAAM.
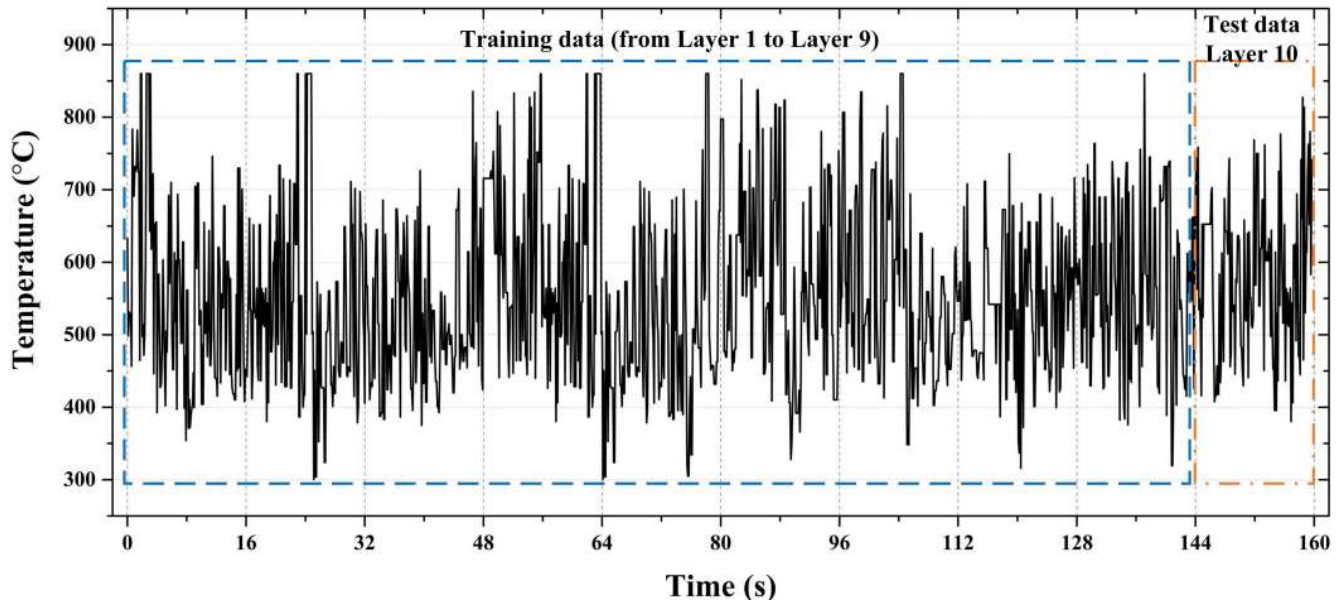
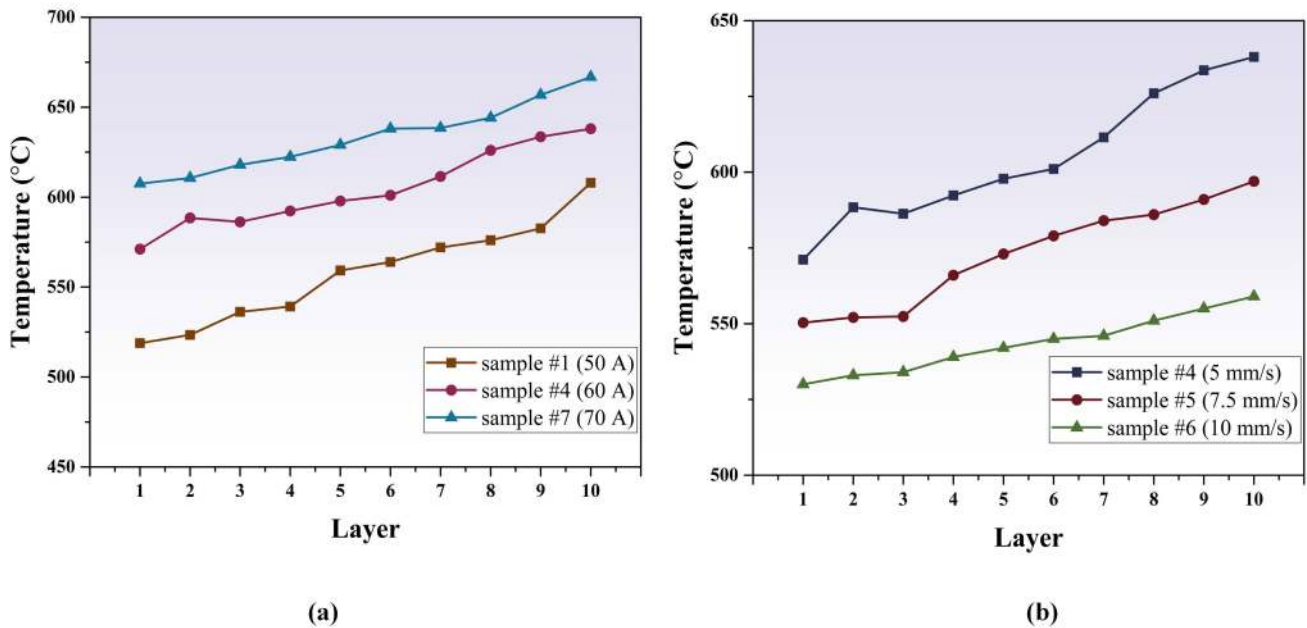**FIGURE 6.** Melt pool temperature distribution of sample 1 (current – 50 A and speed – 5 mm/s).

FIGURE 7. Layer-wise average melt pool temperature versus: (a) current and (b) speed.

Statistical models include exponential smoothing (ETS), autoregressive integrated moving average (ARIMA), linear regression (LR), support vector machines (SVM) and random forests (RF). Optimal hyperparameters were chosen from grid search method. The careful selection of optimal parameters was made in order to achieve the best performance of each model, and compared with the proposed model.

The results obtained for various statistical and machine learning models are shown in Table 6. The RMSE obtained for ETS and ARIMA models are 118.98 and 100.44 respectively. The performance of statistical models lags when compared to the machine learning models. The RMSE of random forest model at 99.25 outperforms other models. Linear regression was performed with degree 2-interaction. The results are quite competitive over ETS, ARIMA and SVM, as can be seen in Fig. 9. However, the superior performance of proposed CNN-LSTM model with high flexibility and repeatability shows
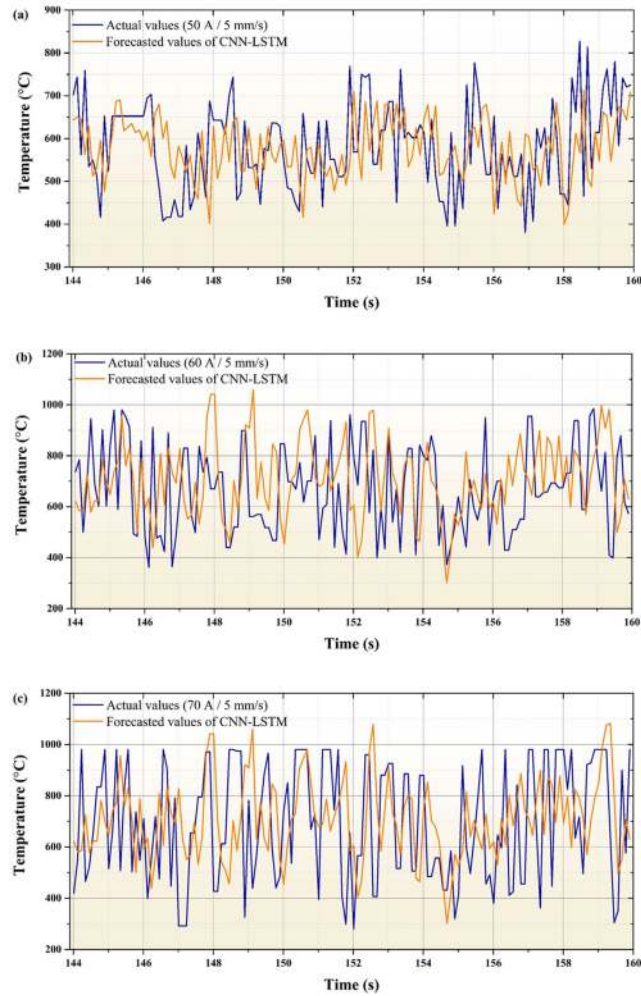
FIGURE 8. Forecasted values of proposed method for three different samples: (a) sample 1, (b) sample 2 and (c) sample 3.
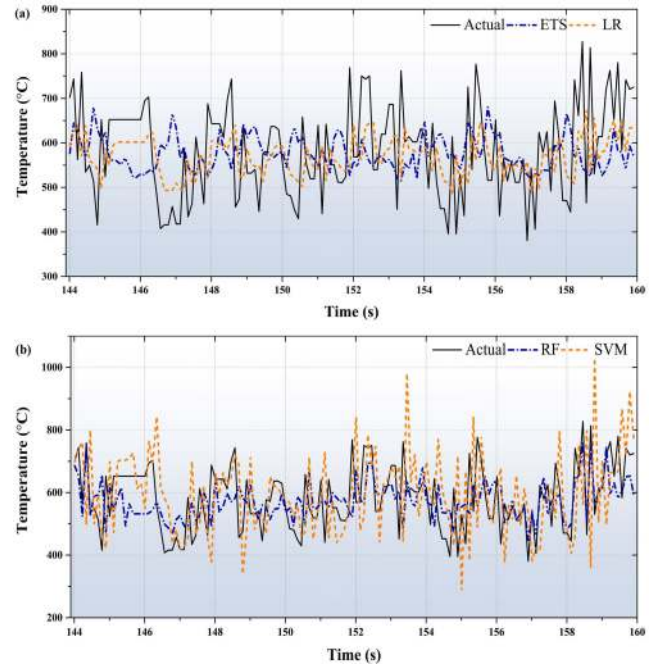

FIGURE 9. Forecasted values of time series models (a) ETS and ARIMA and (b) SVM and RF.

TABLE 5. Parameters setting for statistical and machine learning models.

S.No.	Model	Description
1	ETS	Seasonal periods=100, trend=additive, seasonal=multiplicative
2	ARIMA	(p, d, q) = (6, 0, 2)
3	LR	Two-step, (x1, x2, c) = (0.053, 0.405, 302.42)
4	SVM	Kernel=linear, C=1000, gamma=0.02
5	RF	Number of estimators=100

TABLE 6. Comparative results of various statistical and machine learning models.

Method	RMSE	MAE	MAPE(%)
ETS	118.98	99.28	17.70
ARIMA	100.44	92.67	14.56
LR	102.30	84.51	14.73
SVM	157.10	117.56	20.76
RF	99.25	80.40	14.12

the capability of forecasting melt pool temperature in real-time.

B. PERFORMANCE COMPARISON WITH DEEP LEARNING MODELS

To validate the superior performance of the proposed method, we compared results with other existing deep learning models available for time-series forecasting. The performance metrics of various deep learning models and the method are shown in Table 7. MLP (Multi-layer perceptron), CNN, GRU (gated recurrent unit), LSTM, Bi-LSTM and Attention-LSTM models were chosen for comparative analysis. The results indicated the superior performance of CNN-LSTM method over other deep learning methods for melt pool temperature forecasting. Fig. 10 shows the comparative results of RMSE (10-fold cross-validation) of various deep learning techniques.

The performance measures of the proposed CNN-LSTM method are significantly better than traditional methods. The RMSE value of the proposed model is decreased by 28.5%,

12%, 29.6%, 35.81%, 22.8% and 21.94% over MLP, CNN, GRU, LSTM, Bi-LSTM and Attention-LSTM models respectively. The percentage improvement of the proposed model over other models were calculated using the following formula: $(RMSE_{model} - RMSE_{CNN-LSTM})/RMSE_{model} * 100$. The performance of stand-alone CNN model is slightly better over Bi-LSTM and Attention-LSTM models. Figure 11 shows the forecasted results of stand-alone CNN and LSTM models. However, accuracy of the proposed hybrid model is significantly better than other conventional deep-learning models. From the results obtained for various time-series models (statistical, machine learning and deep learning techniques), the proposed method proves to be a competitive technique
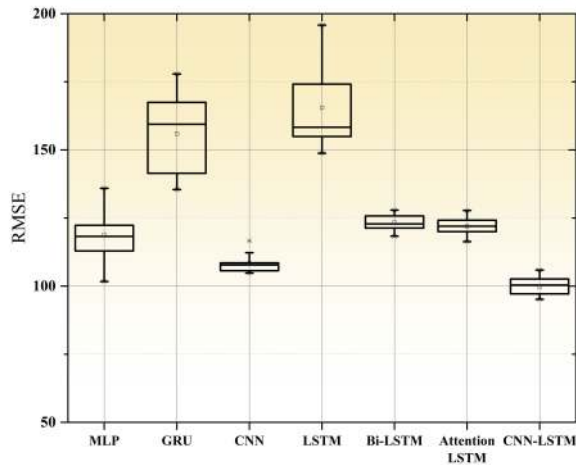
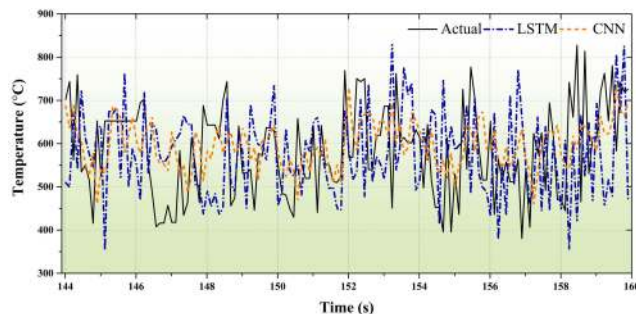**FIGURE 10.** Comparative results of RMSE of deep learning methods (10-fold cross validation).

FIGURE 11. Forecasted values of CNN and LSTM.

TABLE 7. Comparative results of various deep learning models.

Method	RMSE	MAE	MAPE(%)
MLP	133.231	112.97	34.15
CNN	108.521	87.12	15.96
GRU	135.45	100.44	36.68
LSTM	148.757	125.75	22.2
Bi-LSTM	123.32	97.7	31.3
Attention-LSTM	121.92	101.50	28.4
Proposed CNN-LSTM	**95.169**	**75.43**	**12.19**

for real-time melt pool temperature forecasting, and thus for in-situ monitoring.

VI. DISCUSSIONS

The proposed CNN-LSTM network for forecasting melt pool temperature during additive manufacturing process is found to be an effective and competitive technique for online monitoring of process. The existing methods for online monitoring mostly used defect detection techniques such as x-ray, computed tomography measurements that are mapped with temperature profile to adjust process parameters. However, temperature profile itself provides an abundant information regarding the quality of products. Thus, forecasting temperature profile for each layer during additive manufacturing

process is most feasible, by subsequently controlling the process parametric deviations, particularly with higher efficiency and faster response times. Melt pool temperature profile is dynamic and complex in nature. Thus, utilizing stand-alone traditional statistical or machine learning or deep learning models may not be effective. We have improved the forecasting performance by linearly combining CNN and LSTM networks to address the non-linearity from both spatial and sequential point of view.

The comparative results with traditional machine learning models are shown in Table 6. All experiments were performed using 10-fold cross validation approach to maintain generalization for performance comparison. The forecasted results and their comparison with observed values are shown in Fig. 10. We have compared the method with the benchmark statistical, machine learning and deep learning models for melt pool temperature forecasting. Figs. 9 & 11 shows the comparative plots of forecasted values for various machine learning and deep learning techniques. It is observed that the predictions made by the proposed method are better than the conventional models.

The best performance for the proposed model with RMSE of 95.169. Also, the model performed much better than other methods as shown in Tables 6 & 7. The average melt pool temperature obtained for each sample during experimentation is shown in Table 3. The average forecasted melt pool temperature values for the proposed model are 643.86°C, 671.47°C and 696.06°C for 50 A, 60 A and 70 A respectively, while at a constant speed of 5 mm/s. The average forecasted and observed values are close to each other and also smaller standard deviation is observed when compared to other forecasting models. Thus, forecasting results by the proposed method are quite reliable for real-time monitoring of additive manufacturing process.

VII. CONCLUSION

Time-series analysis and forecasting is becoming an important research topic in recent years due to the availability of large amounts of data and high computational power. The present study demonstrated the application of CNN-LSTM model for layer-wise melt pool temperature forecasting during WAAM process. The melt pool temperature of the roof layer (layer 10) is forecasted by training the network with the previous layer's (from layer 1 to layer 9) temperature data. The performance of proposed CNN-LSTM model for all the experiments was evaluated using RMSE, MAE and MAPE. Further, results of proposed model were compared with the traditional benchmark time series models. The major conclusions drawn from this study are the following.

- The performance metrics of CNN-LSTM model for melt pool temperature forecasting followed a similar pattern for all the experiments, that shows the good repeatability of the proposed model.
- The comparative results with traditional models such as ETS, ARIMA, LR, SVM and RF have

shown that the proposed model is capable of forecasting temperature with high accuracy.

- The RMSE value of the proposed model is decreased by 28.5%, 12%, 29.6%, 35.81%, 22.8% and 21.94% over MLP, CNN, GRU, LSTM, Bi-LSTM and Attention-LSTM models respectively.

The right selection of hyperparameters of deep learning models is a major limitation for their general applicability. This usually follows a trial-and-error approach. In future work, inner structure of CNN-LSTM can be extensively studied for further improvement of the model's performance.

REFERENCES

[1] M. Molitch. (Jun. 27, 2020). *Boeing 777x Takes First Flight With Over 600 3D-Printed Parts*. Accessed: Dec. 14, 2020. [Online]. Available https://3dprint.com/262742/boeing-777x-takes-first-flight-with-over-600-3d-printed-parts/

[2] *Standard Guide for Directed Energy Deposition of Metals*, Standard ASTM F3187-16, 2016.

[3] C. R. Cunningham, J. M. Flynn, A. Shokrani, V. Dhokia, and S. T. Newman, "Invited review article: Strategies and processes for high quality wire arc additive manufacturing," *Additive Manuf.*, vol. 22, pp. 672–686, Aug. 2018, doi: 10.1016/j.addma.2018.06.020.

[4] C. G. Pickin, S. W. Williams, and M. Lunt, "Characterisation of the cold metal transfer (CMT) process and its application for low dilution cladding," *J. Mater. Process. Technol.*, vol. 211, no. 3, pp. 496–502, Mar. 2011, doi: 10.1016/j.jmatprotec.2010.11.005.

[5] B. Cong, J. Ding, and S. Williams, "Effect of arc mode in cold metal transfer process on porosity of additively manufactured al-6.3%Cu alloy," *Int. J. Adv. Manuf. Technol.*, vol. 76, nos. 9–12, pp. 1593–1606, Feb. 2015, doi: 10.1007/s00170-014-6346-x.

[6] X. Fang, L. Zhang, H. Li, C. Li, K. Huang, and B. Lu, "Microstructure evolution and mechanical behavior of 2219 aluminum alloys additively fabricated by the cold metal transfer process," *Materials*, vol. 11, no. 5, p. 812, May 2018, doi: 10.3390/ma11050812.

[7] E. M. Ryan, T. J. Sabin, J. F. Watts, and M. J. Whiting, "The influence of build parameters and wire batch on porosity of wire and arc additive manufactured aluminium alloy 2319," *J. Mater. Process. Technol.*, vol. 262, pp. 577–584, Dec. 2018, doi: 10.1016/j.jmatprotec.2018.07.030.

[8] J. Gu, J. Ding, S. W. Williams, H. Gu, P. Ma, and Y. Zhai, "The effect of inter-layer cold working and post-deposition heat treatment on porosity in additively manufactured aluminum alloys," *J. Mater. Process. Technol.*, vol. 230, pp. 26–34, Apr. 2016, doi: 10.1016/j.jmatprotec.2015.11.006.

[9] N. Shamsaei, A. Yadollahi, L. Bian, and S. M. Thompson, "An overview of direct laser deposition for additive manufacturing—Part II: Mechanical behavior, process parameter optimization and control," *Additive Manuf.*, vol. 8, pp. 12–35, Oct. 2015, doi: 10.1016/j.addma.2015.07.002.

[10] L. Tang and R. G. Landers, "Melt pool temperature control for laser metal deposition processes—Part I: Online temperature control," *J. Manuf. Sci. Eng.*, vol. 132, no. 1, Feb. 2010, Art. no. 011010.

[11] T. Lu, C. Liu, Z. Li, Q. Wu, J. Wang, T. Xu, J. Liu, H. Wang, and S. Ma, "Hot-wire arc additive manufacturing Ti–6.5Al–2Zr–1Mo–1 V titanium alloy: Pore characterization, microstructural evolution, and mechanical properties," *J. Alloys Compounds*, vol. 817, Mar. 2020, Art. no. 153334.

[12] P. J. Withers and H. K. D. H. Bhadeshia, "Residual stress. Part 1—Measurement techniques," *Mater. Sci. Technol.*, vol. 17, no. 4, pp. 355–365, Apr. 2001, doi: 10.1179/026708301101509980.

[13] P. J. Withers and H. K. D. H. Bhadeshia, "Residual stress. Part 2—Nature and origins," *Mater. Sci. Technol.*, vol. 17, no. 4, pp. 366–375, Apr. 2001, doi: 10.1179/026708301101510087.

[14] K. S. Derekar, "A review of wire arc additive manufacturing and advances in wire arc additive manufacturing of aluminium ABSTRACT," *Mater. Sci. Technol.*, vol. 34, no. 8, pp. 895–916, 2018, doi: 10.1080/02670836.2018.1455012.

[15] G. Tapia and A. Elwany, "A review on process monitoring and control in metal-based additive manufacturing," *J. Manuf. Sci. Eng.*, vol. 136, no. 6, Dec. 2014, Art. no. 060801.

[16] Y. Xiong, W. H. Hofmeister, Z. Cheng, J. E. Smugeresky, E. J. Lavernia, and J. M. Schoenung, "*In situ* thermal imaging and three-dimensional finite element modeling of tungsten carbide–cobalt during laser deposition," *Acta Mater.*, vol. 57, no. 18, pp. 5419–5429, Oct. 2009, doi: 10.1016/j.actamat.2009.07.038.

[17] S. Cadiou, M. Courtois, M. Carin, W. Berckmans, and P. Le Masson, "3D heat transfer, fluid flow and electromagnetic model for cold metal transfer wire arc additive manufacturing (Cmt-Waam)," *Additive Manuf.*, vol. 36, Dec. 2020, Art. no. 101541, doi: 10.1016/j.addma.2020.101541.

[18] Z. Luo and Y. Zhao, "A survey of finite element analysis of temperature and thermal stress fields in powder bed fusion additive manufacturing," *Additive Manuf.*, vol. 21, pp. 318–332, May 2018, doi: 10.1016/j.addma.2018.03.022.

[19] T. Wuest, D. Weimer, C. Irgens, and K. D. Thoben, "Machine learning in manufacturing: Advantages, challenges, and applications," *Prod. Manuf. Res.*, vol. 4, no. 1, pp. 23–45, Jan. 2016, doi: 10.1080/21693277.2016.1192517.

[20] C. Wang, X. P. Tan, S. B. Tor, and C. S. Lim, "Machine learning in additive manufacturing: State-of-the-art and perspectives," *Additive Manuf.*, vol. 36, Dec. 2020, Art. no. 101538, doi: 10.1016/j.addma.2020.101538.

[21] Z. Zhang, Z. Liu, and D. Wu, "Prediction of melt pool temperature in directed energy deposition using machine learning," *Additive Manuf.*, vol. 37, Jan. 2021, Art. no. 101692, doi: 10.1016/j.addma.2020.101692.

[22] K. Greff, R. K. Srivastava, J. Koutník, B. R. Steunebrink, and J. Schmidhuber, "LSTM: A search space odyssey," *IEEE Trans. Neural Netw. Learn. Syst.*, vol. 28, no. 10, pp. 2222–2232, Oct. 2017, doi: 10.1109/tnnls.2016.2582924.

[23] F. Yu and V. Koltun, "Multi-scale context aggregation by dilated convolutions," in *Proc. 4th Int. Conf. Learn. Represent. (ICLR) Conf. Track*, 2016, pp. 1–13.

[24] I. E. Livieris, E. Pintelas, and P. Pintelas, "A CNN–LSTM model for gold price time-series forecasting," *Neural Comput. Appl.*, vol. 32, no. 23, pp. 17351–17360, Apr. 2020, doi: 10.1007/s00521-020-04867-x.

[25] M. Khanzadeh, S. Chowdhury, L. Bian, and M. A. Tschopp, "A methodology for predicting porosity from thermal imaging of melt pools in additive manufacturing thin wall sections," in *Proc. Additive Manuf., Mater.*, vol. 2, Jun. 2017, Art. no. V002T01A044, doi: 10.1115/msec2017-2909.

[26] U. Sreedhar, C. V. Krishnamurthy, K. Balasubramaniam, V. D. Raghupathy, and S. Ravisankar, "Automatic defect identification using thermal image analysis for online weld quality monitoring," *J. Mater. Process. Technol.*, vol. 212, no. 7, pp. 1557–1566, Jul. 2012, doi: 10.1016/j.jmatprotec.2012.03.002.

[27] J. Mireles, S. Ridwan, P. A. Morton, A. Hinojos, and R. B. Wicker, "Analysis and correction of defects within parts fabricated using powder bed fusion technology," *Surf. Topography, Metrol. Properties*, vol. 3, no. 3, Aug. 2015, Art. no. 034002, doi: 10.1088/2051-672x/3/3/034002.

[28] H. Krauss, C. Eschey, and M. F. Zaeh, "Thermography for monitoring the SLM process," in *Proc. 23rd Annu. Int. Solid Free. Fabr. Symp. Addit. Manuf. Conf. (SFF)*, vol. 66, 2012, pp. 999–1014.

[29] G. Lu, A. Kotousov, and E. Siores, "Elementary mathematical theory of thermal stresses and fracture during welding and cutting," *J. Mater. Process. Technol.*, vols. 89–90, pp. 298–302, May 1999, doi: 10.1016/S0924-0136(99)00036-9.

[30] L. A. Bertram, *A Digital Rykalin Function for Welding*. Oak Ridge, TN, USA: Office of Scientific and Technical Information (OSTI), Dec. 1996, doi: 10.2172/481611.

[31] A. J. Pinkerton and L. Li, "Modelling the geometry of a moving laser melt pool and deposition track via energy and mass balances," *J. Phys. D, Appl. Phys.*, vol. 37, no. 14, pp. 1885–1895, Jul. 2004, doi: 10.1088/0022-3727/37/14/003.

[32] J. Beuth and N. Klingbeil, "The role of process variables in laser-based direct metal solid freeform fabrication," *JOM*, vol. 53, no. 9, pp. 36–39, Sep. 2001, doi: 10.1007/s11837-001-0067-y.

[33] F. Hejripour, D. T. Valentine, and D. K. Aidun, "Study of mass transport in cold wire deposition for wire arc additive manufacturing," *Int. J. Heat Mass Transf.*, vol. 125, pp. 471–484, Oct. 2018, doi: 10.1016/j.ijheatmasstransfer.2018.04.092.

[34] S. Kou, *Welding Metallurgy*. Hoboken, NJ, USA: Wiley, 2003.

[35] J. Zhang, F. Liou, W. Seufzer, and K. Taminger, "A coupled finite element cellular automaton model to predict thermal history and grain morphology of Ti-6Al-4 V during direct metal deposition (DMD)," *Additive Manuf.*, vol. 11, pp. 32–39, Jul. 2016, doi: 10.1016/j.addma.2016.04.004.

[36] M. Khanzadeh, S. Chowdhury, M. Marufuzzaman, M. A. Tschopp, and L. Bian, "Porosity prediction: Supervised-learning of thermal history for direct laser deposition," *J. Manuf. Syst.*, vol. 47, pp. 69–82, Apr. 2018, doi: 10.1016/j.jmsy.2018.04.001.

[37] M. Mozaffar, A. Paul, R. Al-Bahrani, S. Wolff, A. Choudhary, A. Agrawal, K. Ehmann, and J. Cao, "Data-driven prediction of the high-dimensional thermal history in directed energy deposition processes via recurrent neural networks," *Manuf. Lett.*, vol. 18, pp. 35–39, Oct. 2018, doi: 10.1016/j.mfglet.2018.10.002.

[38] C.-J. Huang and P.-H. Kuo, "A deep CNN-LSTM model for particulate matter ($PM_{2.5}$) forecasting in smart cities," *Sensors*, vol. 18, no. 7, p. 2220, 2018, doi: 10.3390/s18072220.

[39] T. Li, M. Hua, and X. Wu, "A hybrid CNN-LSTM model for forecasting particulate matter ($PM_{2.5}$)," *IEEE Access*, vol. 8, pp. 26933–26940, 2020, doi: 10.1109/access.2020.2971348.

[40] T.-Y. Kim and S.-B. Cho, "Predicting residential energy consumption using CNN-LSTM neural networks," *Energy*, vol. 182, pp. 72–81, Sep. 2019, doi: 10.1016/j.energy.2019.05.230.

[41] A. U. Rehman, A. K. Malik, B. Raza, and W. Ali, "A hybrid CNN-LSTM model for improving accuracy of movie reviews sentiment analysis," *Multimedia Tools Appl.*, vol. 78, pp. 26597–26613, Jun. 2019, doi: 10.1007/s11042-019-07788-7.

[42] J. Zhang, Y. Li, J. Tian, and T. Li, "LSTM-CNN hybrid model for text classification," in *Proc. IEEE 3rd Adv. Inf. Technol., Electron. Autom. Control Conf. (IAEAC)*, Oct. 2018, pp. 1675–1680, doi: 10.1109/iaeac.2018.8577620.

[43] Y. Luan and S. Lin, "Research on text classification based on CNN and LSTM," in *Proc. IEEE Int. Conf. Artif. Intell. Comput. Appl. (ICAICA)*, Mar. 2019, pp. 352–355, doi: 10.1109/icaica.2019.8873454.

[44] G. Petmezas, K. Haris, L. Stefanopoulos, V. Kilintzis, A. Tzavelis, J. A. Rogers, A. K. Katsaggelos, and N. Maglaveras, "Automated atrial fibrillation detection using a hybrid CNN-LSTM network on imbalanced ECG datasets," *Biomed. Signal Process. Control*, vol. 63, Jan. 2021, Art. no. 102194, doi: 10.1016/j.bspc.2020.102194.

[45] A. Vidal and W. Kristjanpoller, "Gold volatility prediction using a CNN-LSTM approach," *Expert Syst. Appl.*, vol. 157, Nov. 2020, Art. no. 113481, doi: 10.1016/j.eswa.2020.113481.

[46] Y. LeCun, B. Boser, J. S. Denker, D. Henderson, R. E. Howard, W. Hubbard, and L. D. Jackel, "Backpropagation applied to handwritten zip code recognition," *Neural Comput.*, vol. 1, no. 4, pp. 541–551, 1989, doi: 10.1162/neco.1989.1.4.541.

[47] A. Gavrilov, A. Jordache, M. Vasdani, and J. Deng, "Convolutional neural networks: Estimating relations in the ising model on overfitting," in *Proc. IEEE 17th Int. Conf. Cognit. Informat. Cognit. Comput. (ICCI*CC)*, Jul. 2018, pp. 154–158, doi: 10.1109/icci-cc.2018.8482067.

[48] K. He and J. Sun, "Convolutional neural networks at constrained time cost," in *Proc. IEEE Conf. Comput. Vis. Pattern Recognit. (CVPR)*, Jun. 2015, pp. 5353–5360, doi: 10.1109/cvpr.2015.7299173.

[49] M. Z. Afzal, S. Capobianco, M. I. Malik, S. Marinai, T. M. Breuel, A. Dengel, and M. Liwicki, "Deepdocclassifier: Document classification with deep convolutional neural network," in *Proc. 13th Int. Conf. Document Anal. Recognit. (ICDAR)*, Aug. 2015, pp. 1111–1115, doi: 10.1109/icdar.2015.7333933.

[50] S. Hochreiter and J. Schmidhuber, "Long short-term memory," *Neural Comput.*, vol. 9, no. 8, pp. 1735–1780, 1997, doi: 10.1162/neco.1997.9.8.1735.

PAVAN KUMAR NALAJAM received the bachelor's degree in electrical engineering, in 2013, and the master's degree in manufacturing technology. He is currently pursuing the Ph.D. degree in machine learning applications for manufacturing.

His research interests include machine learning, artificial intelligence, directed energy deposition, and time-series analysis and forecasting.

RAMESH VARADARAJAN (Member, IEEE) received the bachelor's degree in mechanical engineering from the Birla Institute of Technology and Science (BITS), Pilani, in 1983, the AMIE degree in electrical engineering from the Institute of Engineers, India, in 1992, the master's degree in power systems engineering from the Thiagarajar College Of Engineering (TCE), Madurai Kamaraj University, in 1994, and the Ph.D. degree from VIT University, Vellore, India, in 2011.

Prior to academics, he had over seven years of experience in industrial control and automation. He is currently a Professor with the School of Electrical Engineering, VIT University. His current interests include machine learning, artificial intelligence, and manufacturing.

• • •